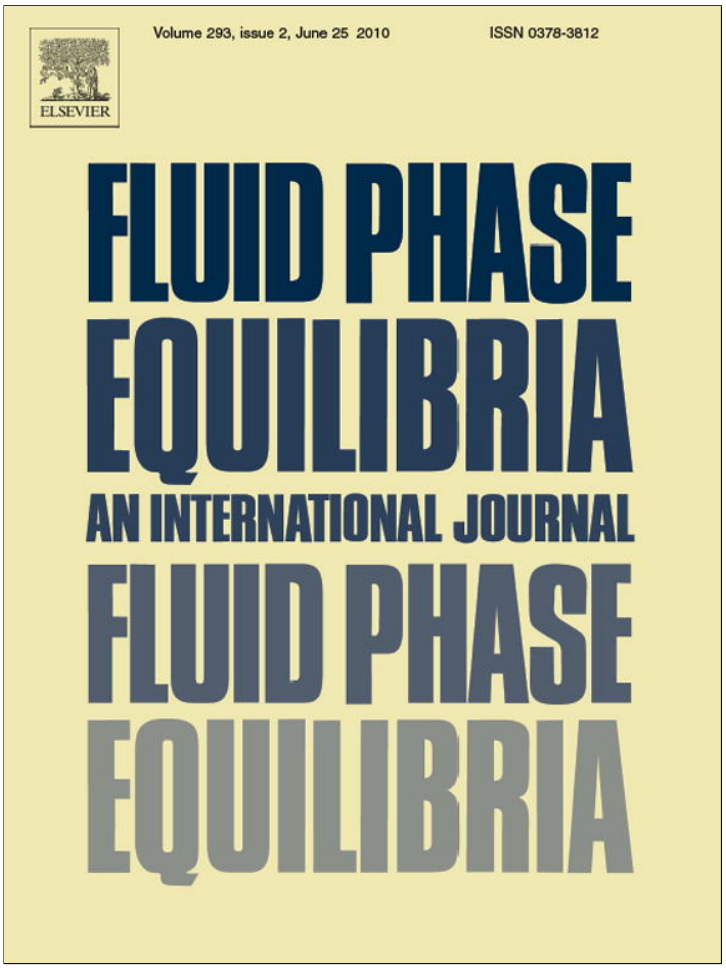

Fluid Phase Equilibria 293 (2010) 196–204

Contents lists available at ScienceDirect

Fluid Phase Equilibria

journal homepage: www.elsevier.com/locate/fluid

Prediction of the transport properties of a polyatomic gas

Zhi Liang, Hai-Lung Tsai*

Department of Mechanical and Aerospace Engineering, Missouri University of Science and Technology (formerly University of Missouri-Rolla), 400 West 13th Street, Rolla, MO 65409, USA

ARTICLE INFO

Article history:
Received 1 September 2009
Received in revised form 4 March 2010
Accepted 6 March 2010
Available online 15 March 2010

Keywords:
Molecular modeling
CO_2
Transport properties
Ab initio

ABSTRACT

An *ab initio* molecular potential model is employed in this paper to show its excellent predictability for the transport properties of a polyatomic gas from molecular dynamics simulations. A quantum mechanical treatment of molecular vibrational energies is included in the Green and Kubo integral formulas for the calculation of the thermal conductivity by the Metropolis Monte Carlo method. Using CO_2 gas as an example, the fluid transport properties in the temperature range of 300–1000 K are calculated without using any experimental data. The accuracy of the calculated transport properties is significantly improved by the present model, especially for the thermal conductivity. The average deviations of the calculated results from the experimental data for self-diffusion coefficient, shear viscosity, thermal conductivity are, respectively, 2.32%, 0.71% and 2.30%.

1. Introduction

To successfully predict transport properties of real fluids from molecular simulation, the most critical problem is to develop an accurate interaction potential model. For polyatomic molecules, a widely used potential model is to represent the intermolecular interactions by multi-center Lennard–Jones plus either quadrupole or dipole moments. The parameters in this potential model were normally adjusted or optimized to experimental vapor–liquid equilibria data [1–4]. These potential models usually predict static thermodynamic properties more accurately than transport properties. To get better transport properties predictions, transport properties need to be used directly in the parameterization of the molecular potential [5]. Therefore, the predictions of transport properties by these potential models strongly depend on the existence and accuracy of the experimental data. In the last decades, with the increasing computing power, accurate determinations of intermolecular potential of polyatomic molecules by *ab initio* methods become feasible. As an example, it was found from the *ab initio* calculation [6] that the CO_2 molecule is a linear molecule with the C–O bond length $r_0 = 1.162$ Å which agrees with the experimental result [7]. Based on the linear molecular structure, a number of potential surfaces have been proposed for CO_2–CO_2 interaction [8–10]. They were all determined by *ab initio* methods and validated by comparing with experimental second virial coefficients. The accurate *ab initio* potentials make it possible to predict a variety of physical properties of fluids without using any experimental data. Once the accurate intermolecular potential is available, appropriate molecular simulation techniques should be employed to calculate the required fluid transport properties. There exist two standard methodologies, i.e., equilibrium molecular dynamics (EMD) which is based on the Einstein relations or Green–Kubo integral formulas [11–13] and non-equilibrium molecular dynamics (NEMD) in which the transport properties are measured by creating a flow in the fluid under study [14]. A lot of researchers prefer using NEMD because NEMD simulations were considered to be more efficient [15–18]. However, NEMD simulations are normally able to provide only one transport property at once [14], whereas EMD is a multi-property method. The thermodynamic properties and transport properties such as self-diffusion coefficient, viscosity and thermal conductivity can be all obtained from the output of a single equilibrium run. Moreover, when an anisotropic potential is used for the calculations of transport properties of a polyatomic gas, the molecular model is much more complicated than the isotropic Lennard–Jones molecular model. In this case, the overall efficiency of non-equilibrium methods is not necessary to be higher than the equilibrium simulations allowing for the need to extrapolate the non-equilibrium simulation results to thermodynamic equilibrium [19]. Therefore, EMD simulations are used in this work.

Although both *ab initio* potential of CO_2 molecules and molecular simulation techniques exist, most of the researchers only used the *ab initio* potential to validate phase equilibrium properties of carbon dioxide [9,20,21]. The amount of calculations of transport properties such as viscosity and thermal conductivity based on the *ab initio* potential is scarce. On the other hand, there are several calculations of CO_2 transport properties based on potential models

* Corresponding author. Tel.: +1 573 341 4945; fax: +1 573 341 4607.
E-mail address: tsai@mst.edu (H.-L. Tsai).

0378-3812/$ – see front matter © 2010 Elsevier B.V. All rights reserved.
doi:10.1016/j.fluid.2010.03.007

optimized to experimental data [3,18,22]. However, the deviations between the simulated results and experimental data still reached 10% for self-diffusion coefficient [22], 5% for shear viscosity and 10% for thermal conductivity at low temperature and high densities [3]. A deviation of up to 30% was even found for thermal conductivities at relatively high temperature and low densities [18]. The large deviations are mainly caused by not sufficient accurate potential and inappropriate treatment of molecular vibrations. The purpose of the present work is to use CO_2 gas as an example to demonstrate that if quantum effects of molecular vibrations are treated appropriately, the self-diffusion coefficient, shear viscosity and thermal conductivity of a polyatomic gas in a wide range of temperature can all be accurately determined from EMD simulations by employing an *ab initio* potential. The three transport properties of CO_2 gas at 1 atm and in the temperature range of 300–1000 K are calculated in this work. In this range of temperatures, accurate experimental data are available and can be used to validate the calculation method and the *ab initio* potential employed in the work.

The *ab initio* potential surfaces proposed for carbon dioxide all treated CO_2 molecules as linear rigid rotors. Hence, in this work we assume the structure of CO_2 is unaffected by the interaction between molecules. The self-diffusion coefficient and shear viscosity measure the transports of mass and momentum in the fluid. The influence of vibrational motions can be neglected in those calculations since the transfer of vibrational energy to rotational and translational degrees of freedom is extremely slow [9] and the vibrational energy can be considered as frozen in the molecule in the simulation. The thermal conductivity, however, measures the transport of energy through the fluid. Hence, the vibrational energy must be considered in the calculation of thermal conductivity.

Based on the above assumptions, the MD simulations are carried out in the microcanonical ensemble. The statistical errors in the calculations of the time correlation functions are inversely proportional to the square root of the simulation length. To obtain a relative precision of less than 1% in the time correlation function, it is necessary to conduct a run of 10^4 correlation time [23]. An estimation based on the preliminary results in this work shows the correlation time for a CO_2 gas in the temperature range of 300–1000 K is in the order of 10^2 ps. Hence, long simulations up to the order of 10 μs are required to obtain accurate results. To save the total computational cost, the original *ab initio* potential is employed with a small modification so that large time step sizes can be used without causing the energy conservation problem.

This paper is organized as follows. The following section provides the theoretical background of Green–Kubo formula. In Section 3, the modified *ab initio* intermolecular potential and force are presented. In Section 4, we describe the MC method used for initializing the MD simulations. The results of the MD simulations compared to experimental results are given in Section 5. Finally, the conclusions are drawn in Section 6.

2. Theoretical background

In the time-correlation function theory, the three transport properties considered can be all calculated by either the Green–Kubo integral formulas or the Einstein–Helfand relations in equilibrium simulations. It can be proven [24] that the Einstein–Helfand relations are equivalent to the Green–Kubo formulas. However, due to the periodic boundary conditions (PBCs) used in MD simulations, the original expressions of the Einstein–Helfand relations cannot be applied directly. Also, additional terms must be included allowing for discontinuous particle trajectories in a finite-system simulation with PBCs [25]. Hence, in this work we use the Green–Kubo formulas.

The Green–Kubo formula for self-diffusion coefficient D can be expressed as [14]

$$D = \frac{1}{3}\int_0^\infty dt \langle \vec{v}_i(t)\cdot\vec{v}_i(0)\rangle, \tag{1}$$

where $\vec{v}_i$ is the translational velocity of ith molecule; t is the time; and $\langle\cdots\rangle$ denotes ensemble average. To improve statistical accuracy, the velocity time correlation function is computed by averaging over 1000 molecules in the simulation.

The shear viscosity η given by the Green–Kubo formula is [14]

$$\eta = \frac{V}{k_B T}\int_0^\infty dt \langle P_{\alpha\beta}(t)\cdot P_{\alpha\beta}(0)\rangle, \tag{2}$$

where

$$P_{\alpha\beta} = \frac{1}{V}\left(\sum_i m v_{i\alpha} v_{i\beta} + \sum_i\sum_{j>i} r_{ij\alpha} f_{ij\beta}\right). \tag{3}$$

In Eqs. (2) and (3), the subscript α and β denote the vector component. Due to the PBCs used in the simulation, the minimum-image convention is employed to find all interacting pairs. Since the viscosity is a multi-particle property, no additional averaging over the N particles is possible to improve the statistical accuracy. The viscosity, therefore, requires much longer simulations than the self-diffusion coefficient to get accurate results.

The Green–Kubo formula relates the thermal conductivity λ_T to the time autocorrelation function of the energy current via the following relation [14]

$$\lambda_T = \frac{V}{k_B T^2}\int_0^\infty dt \langle J_\alpha(t) J_\alpha(0)\rangle. \tag{4}$$

Here, J_α is a component of the energy current, i.e., the time derivative of

$$\delta E = \frac{1}{V}\sum_i r_{i\alpha}(E_i - \langle E_i\rangle). \tag{5}$$

It is shown in the Appendix A that J_α can be expressed as

$$J_\alpha = \frac{1}{V}\left(\sum_i v_{i\alpha} E_i + \sum_i\sum_{j>i} r_{ij\alpha}\frac{dE_{ij}}{dt}\right), \tag{6}$$

where E_i is the energy of the molecule i which contains the translational, rotational, vibrational and intermolecular potential energies

$$E_i = \frac{1}{2}m v_i^2 + \frac{1}{2}I u_i^2 + E_{Vi} + \frac{1}{2}\sum_{j\neq i} U_{ij}, \tag{7}$$

and dE_{ij}/dt represents the time rate of the change of the energy in the molecule i due to the interactions between molecule i and molecule j which can be expressed as

$$\frac{dE_{ij}}{dt} = \frac{1}{2}(\vec{v}_i + \vec{v}_j)\cdot\vec{F}_{ij} + \frac{1}{2}(\vec{u}_i\cdot\vec{G}_{ij}^{\perp} - \vec{u}_j\cdot\vec{G}_{ji}^{\perp}). \tag{8}$$

In Eq. (7), I and m are, respectively, the moment of inertia and mass of the CO_2 molecule; E_{Vi} and U_{ij} are, respectively, the vibrational energy of the molecule i and the intermolecular potential energy between the molecule i and molecule j. The vibrational energies in Eq. (7) cannot be neglected especially for polyatomic molecules like CO_2 which contain low-lying vibrational states. In Eq. (8), $\vec{u}_i$ is the rotational velocity of the molecule i which is defined as $\dot{\vec{e}}_i$ the time derivative of the unit vector along the molecular axis. $\vec{G}_{ij}^{\perp}$ can be determined from the intermolecular forces by Eq. (9)

$$\vec{G}_{ij} = \sum_a d_{ia}\vec{f}_{ija}, \tag{9}$$

where d_{ia} is the distance of the site a in the molecule i relative to the center of mass. $\vec{f}_{ija}$ is the force acting on the site a in the molecule i due to the interaction between the molecule i and molecule j. $\vec{G}_{ij}^{\perp}$ is the component of $\vec{G}_{ij}$ perpendicular to $\vec{e}_i$, i.e., the axis of the molecule i. Each time autocorrelation function is averaged over the autocorrelation functions of the energy currents in three directions, i.e., J_x, J_y, and J_z to reduce the statistical uncertainty of the calculated thermal conductivity.

Due to the interactions among molecules in the system, the translational, rotational and intermolecular potential energies all vary with time. However, the vibrational energies are assumed as frozen in the molecules so that they have no influence on the molecular interactions.

3. Intermolecular potential

The intermolecular potential employed in the work was proposed by Bukowski et al. (BUK) [8]. The BUK potential was computed using the many-body symmetry-adapted perturbation theory (SAPT) and a large 5s3p2d1f basis set. In addition to BUK potential, there are two more *ab initio* potentials proposed for the carbon dioxide dimer which were proved to have good qualities. One is Steinebrunner et al. potential based on the MP2 level of theory including corrections for basis set superposition error [9]. Strictly speaking, the Steinebrunner et al. potential is not a pure *ab initio* potential because the original *ab initio* potential was scaled by a parameter of 1.16 in order to obtain a good agreement with experimental second virial coefficients. In this work, we would like to predict the transport properties without any experimental data. Hence, the scaled Steinebrunner et al. potential is not employed here. The other potential was proposed by Bock et al. [10]. Bock et al.'s potential was calculated with the supermolecular approach on MP2 level of theory including full counterpoise corrections. The shapes of Bock et al. potential and the BUK potential are practically the same. They both used a site–site representation of the intermolecular potential, but in different analytical forms. From our preliminary tests, the application of the Bock et al.'s potential is more time-consuming in the calculations of intermolecular potentials and forces than that of the BUK potential. To save computational time, the BUK potential is employed in this work.

The site–site fit BUK potential reads

$$U_{\mathrm{BUK}} = \sum_{a\in \mathrm{A}}\sum_{b\in \mathrm{B}} \left[\exp(\alpha_{ab} - \beta_{ab} r_{ab}) + f_1(\delta_1^{ab} r_{ab}) \frac{q_a q_b}{r_{ab}} - f_6(\delta_6^{ab} r_{ab}) \frac{C_6^{ab}}{r_{ab}^6} - f_8(\delta_8^{ab} r_{ab}) \frac{C_8^{ab}}{r_{ab}^8} \right], \quad (10)$$

where

$$f_n[x] = 1 - e^{-x} \sum_{k=0}^{n} \frac{x^k}{k!}. \quad (11)$$

Here, sites a belong to monomer A, sites b belong to monomer B and r_{ab} is the distance between a and b. Each monomer contained five sites, with three corresponding to the centers of the atoms in CO_2 and the remaining two on the C–O bonds 0.8456 Å away from the C atom. Parameters α_{ab}, β_{ab}, δ_n^{ab}, q_a, and C_n^{ab} are given in Ref. [8].

Fig. 1 shows the shapes of the BUK potential for the parallel configuration and the slipped parallel configuration. Although the potential always tends to approach to zero at large intermolecular distances, it could be either a positive or a negative value around zero depending on the relative orientations of two molecules as shown in Fig. 1. Hence, a truncation and shifted procedure is not applicable to the BUK potential no matter the cut-off criterion is based on distance or energy. Hence, the original BUK potential is

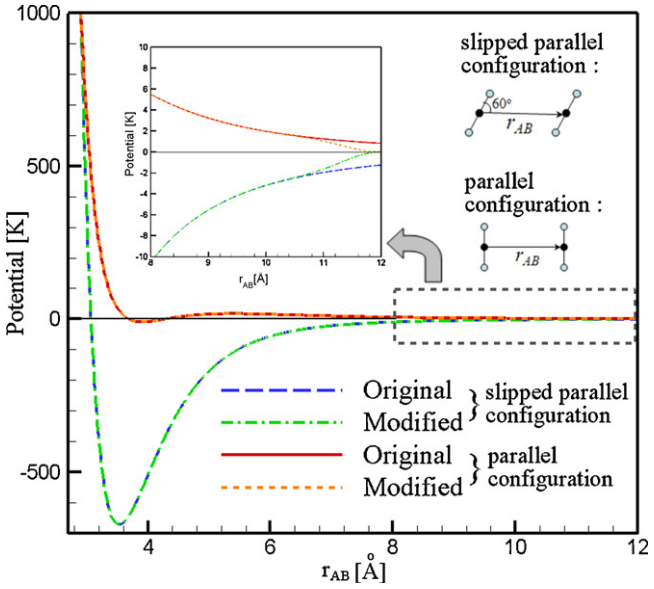

Fig. 1. The shapes of the original and modified BUK intermolecular potential for parallel configuration and slipped parallel configuration.

modified as follows

$$U_{\mathrm{AB}} = \begin{cases} U_{\mathrm{BUK}} \cdot \left[1 - e^{(r_{\mathrm{AB}} - r_{\mathrm{cut}})^2 / -2.0}\right] & r_{\mathrm{AB}} \le r_{\mathrm{cut}} \\ 0 & r_{\mathrm{AB}} > r_{\mathrm{cut}} \end{cases}, \quad (12)$$

where r_{AB} is the intermolecular distance and r_{cut} is the cut-off distance. Both r_{AB} and r_{cut} are in atomic units. In this work, we set r_{cut} = 12 Å. With such a large cut-off distance, the use of an Ewald sum to treat long range Coulomb interactions is not necessary [9,21] which is assisted by the fact that CO_2 molecules are neither charged nor have a permanent dipole moment. The modified potential makes the intermolecular potential go smoothly to zero at the cut-off distance.

The modified potential also ensures the continuity of the intermolecular forces near the cut-off distance. In addition to the forces acting on five sites of each molecule, there is one more force acting on the center of mass of the molecule as shown below

$$\vec{F}(\vec{r}_{\mathrm{AB}}) = U_{\mathrm{BUK}} \cdot \left[-(r_{\mathrm{AB}} - r_{\mathrm{cut}}) e^{(r_{\mathrm{AB}} - r_{\mathrm{cut}})^2 / -2.0} \frac{\vec{r}_{\mathrm{AB}}}{r_{\mathrm{AB}}} \right], \quad (13)$$

In a CO_2 molecule, the center of mass happens to be the carbon atom. Hence, this additional force is actually acting on the carbon atom. Using the modified potential, the forces and torques acting on molecules both go smoothly to zero at the cut-off distance. Thus, the problems in energy conservation and numerical instability in the equations of motion are both eliminated by the modified potential. A simple test of the modified potential shows the second virial coefficient calculated from the modified BUK potential at 300 K is only 0.4% higher than that calculated from the original truncated BUK potential. Hence, the macroscopic properties calculated from the modified BUK potential will not significantly deviate from the corresponding properties from the original potential.

4. Initialization and equilibration

Before attempting to compute proper simulation averages, the system must be equilibrated to both configuration and velocity

distributions appropriate to a gas at the desired temperature and pressure. To save the simulation time for the equilibration process, the configuration of centers of mass and molecular orientations, the translational and rotational velocities should all be initialized at the desired temperature and pressure so that they can relax quickly to the appropriate configuration and velocity distributions.

4.1. The initial configuration and initial energies

The volume of the cubic simulation box is initialized by the ideal gas law

$$V = \frac{Nk_BT}{P}, \tag{14}$$

where P and T are the desired pressure and temperature of the gas; $N = 4096$ is the number of molecules in the system which has the same value in all simulations in this work. The center of mass coordinates $\vec{r}$ is initialized randomly inside the simulation box. The molecular orientations are initialized as random vectors with uniform solid angle.

The initial translational and rotational velocities are given by the Maxwell–Boltzmann distribution at a given temperature. Different from translational and rotational motions, the quantum effects of molecular vibrational motions cannot be neglected. The CO_2 molecule has four vibrational modes. The corresponding vibrational energy eigen values can be determined by solving the rovibrational Schrödinger equation of the molecule. To solve the rovibrational Schrödinger equation, it is necessary to calculate the intramolecular potential energy surface (PES) by *ab initio* method. An accurate CO_2 intramolecular PES has been calculated by Leonard et al. [26] using the coupled-cluster singles and doubles excitation with perturbative treatment of triple excitations method and the multi-reference configuration interaction method. Based on this result, the calculated vibrational energy eigen values corresponding to the 1st excited states of the symmetric stretching mode, the asymmetric stretching mode and the doubly degenerated bending mode are 1387.9 cm^{-1}, 2348.8 cm^{-1} and 667 cm^{-1}, respectively. Although the energy differences between any two neighboring energy states of each vibrational mode are not exactly constant due to the aharmonic component of the intramolecular potential and the Fermi resonance between different vibrational modes, we can still assume the vibrational energies of each mode are equally spaced without causing too much error in the calculations of thermal properties of CO_2 gas. Based on the quantum harmonic oscillator assumption, the vibrational energy of each molecule can be calculated by Eq. (15)

$$E_V = \sum_{j=1}^{4} \left(n_j + \frac{1}{2}\right) E_{vj}, \tag{15}$$

where n_j means the vibrational energy level of jth vibrational mode; E_{vj} is the fundamental vibrational transition energy of mode j.

The average population distribution of vibrational energies fulfills the Boltzmann distribution. At a given temperature, the molecular vibrational energies are initialized by the Metropolis MC method [27]. At the beginning of the initialization, all molecules are on their ground vibrational energy states. Then, the Metropolis scheme is applied to each vibrational mode of each molecule in the system so that the molecules may be excited to higher energy states or decay to lower energy states. After tens of trial transitions, the average vibrational energy per molecule in the system started to fluctuate around a constant value as shown in Fig. 2. The fluctuating average vibrational energies correspond to different distributions of vibrational energies in the molecules. The average of these distributions is the Boltzmann distribution at the given temperature. Two thousands of these distributions are used to initialize the vibrational energies of the molecules in the system. Hence, each MD simulation actually starts with 2000 different initial vibrational energy distributions but with the same initial configuration and initial translational and rotational velocities. Once the vibrational energies are initialized, they do not change during the simulation. Therefore, 2000 time correlation functions of the energy current corresponding to 2000 different initial vibrational energy distributions are obtained from each MD simulation. These time correlation functions calculated from different initial states are then averaged to determine the final time autocorrelation function at the given temperature.

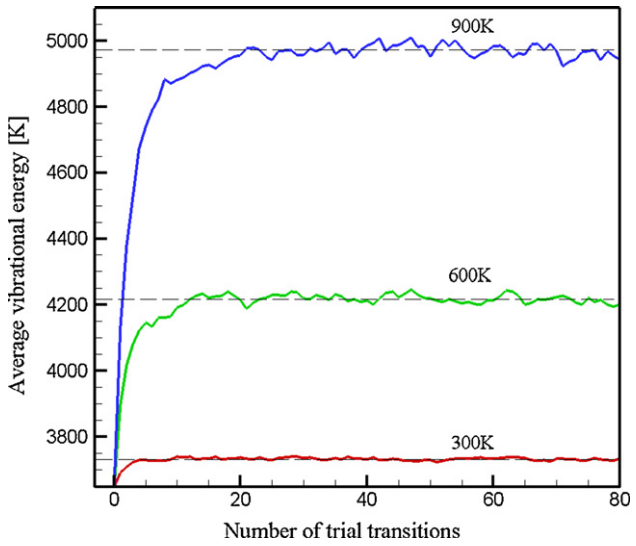

Fig. 2. The average vibrational energy per molecule vs. the number of trail transitions at 300 K, 600 K and 900 K.

4.2. Equilibration

To equilibrate the system to the desired temperature and pressure, the system is coupled to a constant temperature and pressure bath using the approach proposed by Berendsen et al. [28]. At each

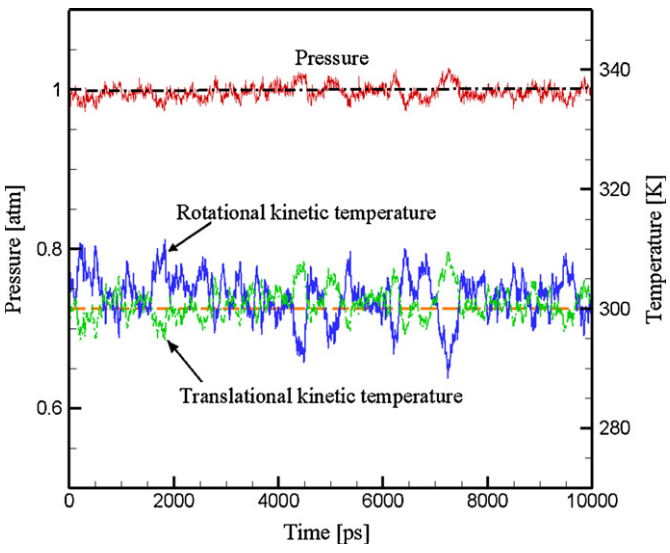

Fig. 3. Translational, rotational kinetic temperatures and pressure vs. time when the equilibrium temperature and pressure are 300 K and 1 atm.

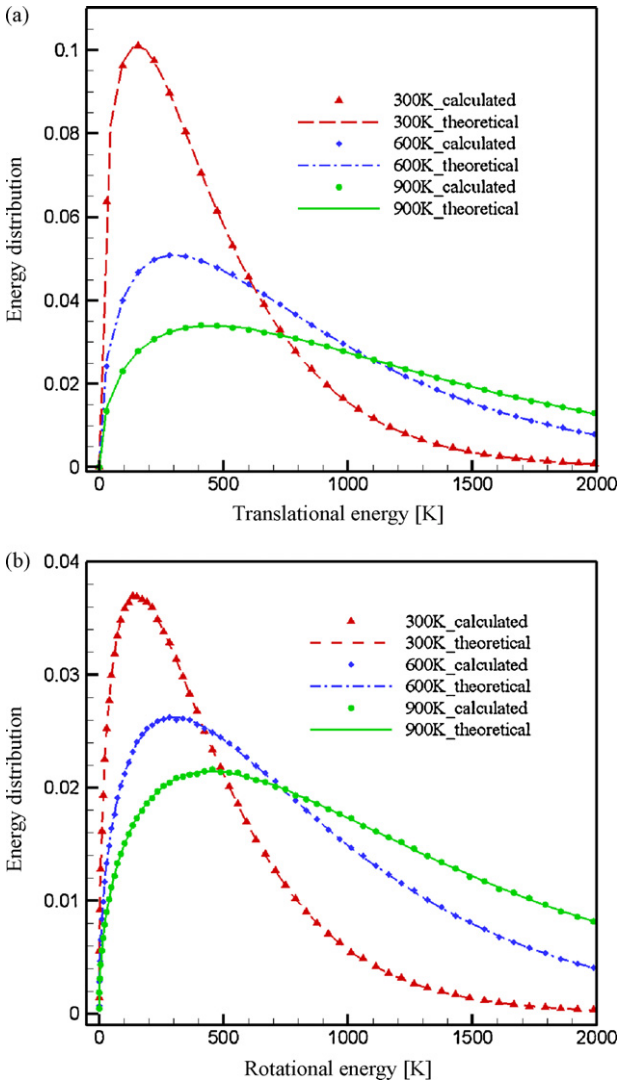

Fig. 4. The calculated and theoretical energy distributions at 300 K, 600 K, and 900 K for (a) translational energies and (b) rotational energies.

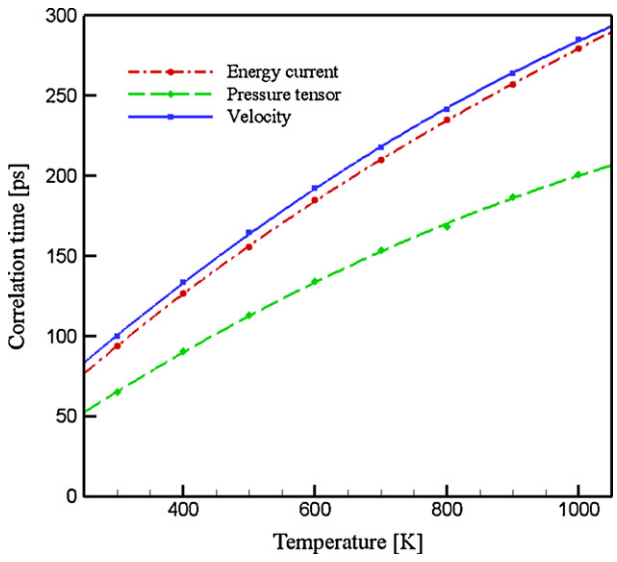

Fig. 5. The correlation times vs. temperature.

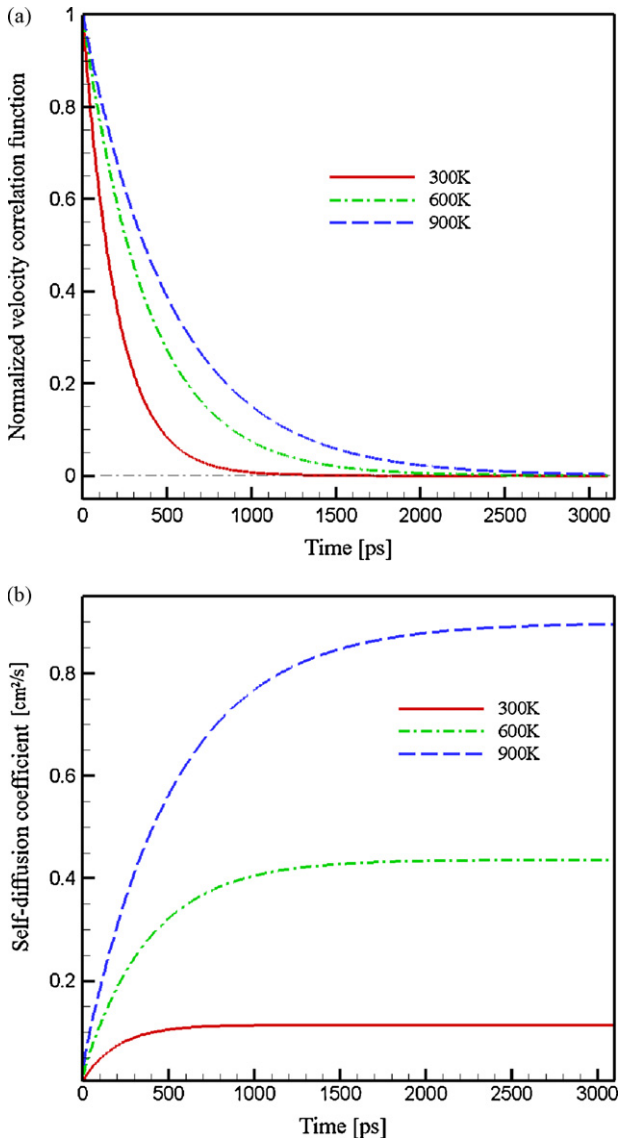

Fig. 6. (a) Normalized velocity correlation functions for selected temperatures. (b) The time integrals of the correlation functions for selected temperatures.

time step, translational velocities are scaled by a factor

$$\lambda = \left[1 + \frac{\Delta t}{\tau_T}\left(\frac{T_0}{T} - 1\right)\right]^{1/2}, \tag{16}$$

where T_0 is the desired temperature varying from 300 K to 1000 K; T is the current translational temperature; Δt is the time step; and τ_T is a preset time constant. The energy exchanges between the translational motion and rotational motion are fast. Hence, the scale factor can force both translational and rotational kinetic temperatures to the desired temperature. Simultaneously, the molecular center of mass coordinates is scaled by a factor of μ, and the volume of the simulation box is scaled by a factor of μ^3 where

$$\mu = \left[1 + \frac{\Delta t}{\tau_p}\beta_T(P - P_0)\right]^{1/3}. \tag{17}$$

Here, P_0 is the desired pressure which is equal to 1 atm in this work; P is the instantaneous pressure; τ_p is a time constant; and β_T is the isothermal compressibility. Since $\beta_T \approx 1/P_0$ for a gas, Eq. (17)

Table 1
The calculated and experimental values [32,33] of self-diffusion coefficient and shear viscosity of CO_2 gas at 1 atm and in the temperature range of 300–1000 K. The deviations (%) are determined by |calculated value − experimental value|/experimental value × 100. The experimental self-diffusion coefficients are obtained by linear interpolation of experimental data in Ref. [33]. Statistical uncertainty of the simulation results is 0.1% for self-diffusion coefficient and 1% for both shear viscosity and thermal conductivity.

	Self-diffusion coefficient D (cm^2/s)			Shear viscosity η (μPa s)			Thermal conductivity λ_T (W/m K)		
	Calculated	Experimental	% Deviation	Calculated	Experimental	% Deviation	Calculated	Experimental	% Deviation
300 K	0.1142	0.1192	4.19	15.34	15.13	1.39	0.01646	0.01679	1.97
400 K	0.2028	0.2063	1.70	19.79	19.70	0.46	0.02445	0.02514	2.74
500 K	0.3116	0.3103	0.42	23.91	24.02	0.46	0.03237	0.03350	3.37
600 K	0.4358	0.4299	1.37	28.51	28.00	1.82	0.04041	0.04156	2.77
700 K	0.5771	0.5640	2.32	31.90	31.68	0.69	0.04851	0.04930	1.60
800 K	0.7310	0.7123	2.63	35.06	35.09	0.09	0.05536	0.05671	2.38
900 K	0.8976	0.8725	2.88	38.18	38.27	0.24	0.06185	0.06380	3.06
1000 K	1.0770	1.0448	3.06	41.04	41.26	0.53	0.07034	0.07057	0.57

can be rewritten as

$$\mu = \left[1 + \frac{\Delta t}{\tau_p}\left(\frac{P}{P_0} - 1\right)\right]^{1/3}. \quad (18)$$

In the simulations, the time constants τ_T and τ_p are set to be 100 ps and 30 ps, respectively. At 1 atm, the long range correction to the pressure of CO_2 gas is negligible. Thanks to all these methods we use in the initialization and equilibration, the system is well equilibrated in 500 ps. After the system reaches the thermal equilibrium at the desired temperature and pressure, the coupling to the external bath is turned off and the MD simulation is carried out in a microcanonical ensemble. The translational temperature, the rotational kinetic temperature, and the pressure of the system all fluctuate around the desired values during the simulation as shown in Fig. 3. The energy exchange between the translational and rotational motions is evident. Fig. 4(a) and (b) depicts the distributions of translational energy and rotational energy obtained from simulations and the corresponding Boltzmann energy distributions at the desired temperature. The good agreement between the calculated results and the theoretical results proves the system is in thermodynamic equilibrium.

5. Simulation details and results

We carried out MD simulations in microcanonical ensembles for pure CO_2 gas in the temperature range of 300–1000 K to calculate the self-diffusion coefficients, shear viscosity and thermal conductivity. The equations of molecular translational motions are integrated by the Verlet leap-frog algorithm. The Singer leap-frog algorithm [29] which constrains the bond length to be a constant is applied to integrate the equations of molecular rotational motions. The modified BUK potential is used for molecular interactions. Compared to the standard LJ potential, the BUK potential has a much more complex form. Therefore, the calculations of forces and potentials are much more time-consuming. To ensure the time step size does not significantly influence the results for the macroscopic properties of the system, the total energy of the system should be kept constant within two parts in 10^5 [30]. Thanks to the modified BUK potential, a time step of 12.5 fs can be used for low temperatures up to 500 K and a 10-fs time step is appropriate for the gas temperature up to 800 K. For higher temperatures, smaller step size of 8.5 fs should be chosen to assure the energy conservation.

The correlation time t_c for the three properties of interest can be calculated by Eq. (14) [23]

$$t_c = \frac{\int_0^\infty dt\ \langle A(0)A(t)\rangle^2}{\langle A^2(0)\rangle^2}, \quad (19)$$

where $A = \vec{v}_i$ for self-diffusion coefficient; $A = P_{\alpha\beta}$ for shear viscosity; and $A = J_\alpha$ for thermal conductivity. Fig. 5 shows the relation between the correlation times and temperature. It can be seen from Fig. 5 that the velocity correlation times are close to the energy current correlation times and are about 50% higher than the correlation time of off-diagonal element of pressure tensor in the temperature range from 300 K to 1000 K. The correlation times of CO_2 gas are generally on the order of 100 ps. The total simulation length of

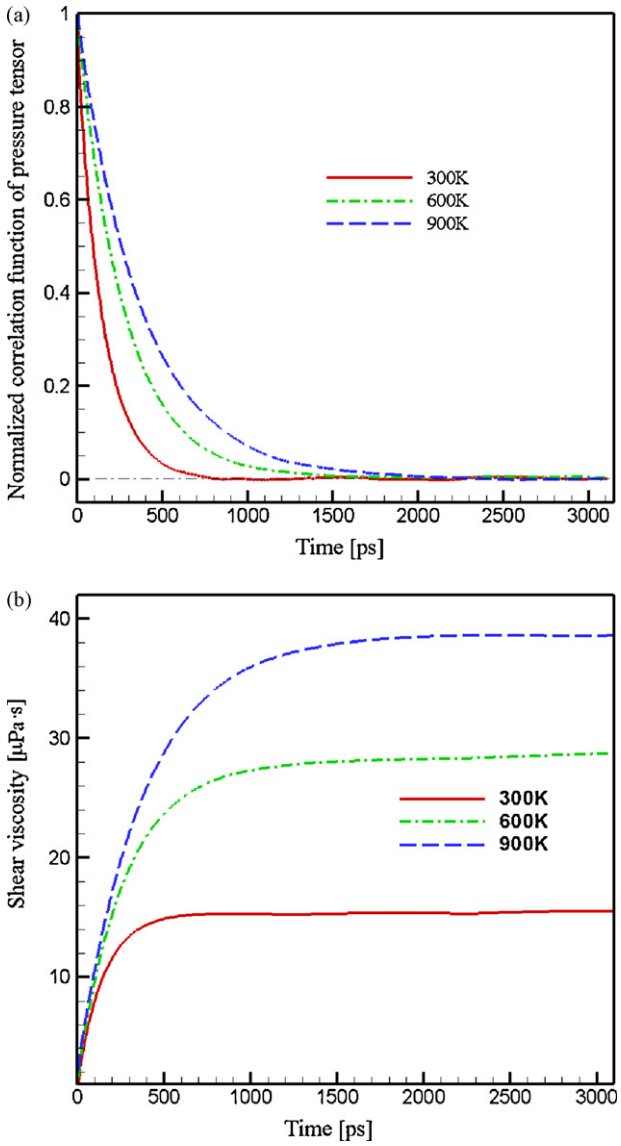

Fig. 7. (a) Normalized correlation functions of off-diagonal elements of pressure tensors for selected temperatures. (b) The time integrals of the correlation functions for selected temperatures.

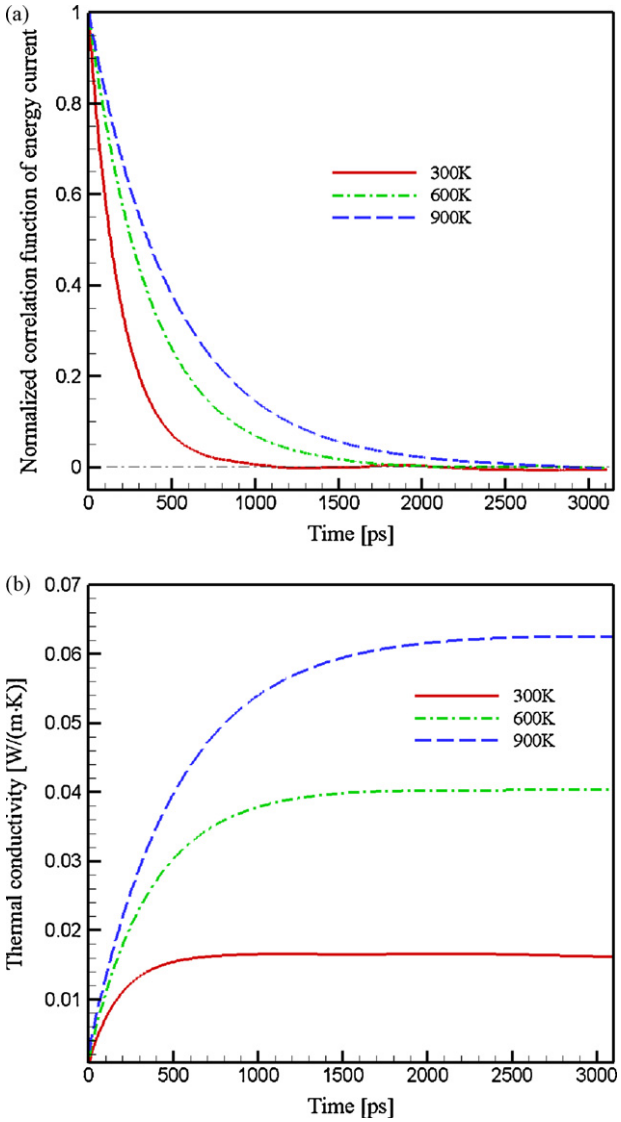

Fig. 8. (a) Normalized correlation functions of energy current at 300 K, 600 K and 900 K. (b) The time integral of the autocorrelation functions for selected temperatures.

order 10 μs, therefore, must be run in order to reduce the statistical errors to less than 1%. If the time step is 10 fs, the total number of steps is about 10^9. This means a very computational demanding simulation is required. As suggested by Hess and Evans [31], the ensemble average can also be obtained from shorter parallel runs starting from statistically independent initial states. Hence, at each temperature, the long simulation is divided into 100 shorter parallel runs which are independently initialized and equilibrated at the given temperature by the method described in Section 4. Depending on the temperature of the system (300–1000 K), the length of each parallel run varies between 60 ns and 140 ns to assure low statistical errors. The final time correlation functions are obtained by averaging the time correlation functions calculated from shorter parallel runs.

Figs. 6(a), 7(a) and 8(a) depict, respectively, the calculated normalized correlation functions of the velocity, the off-diagonal element of pressure tensor and the energy current at 300 K, 600 K and 900 K. The self-diffusion coefficients D, shear viscosities η and thermal conductivities λ_T are determined by the time integrals of the corresponding correlation functions. The results are depicted, respectively, in Figs. 6(b), 7(b) and 8(b). After $10t_c$, no significant contribution to time integrals of correlation functions is observed and the integrals fluctuate around a constant. We evaluate the three transport properties by the averages of those fluctuating values between $10t_c$ and $30t_c$ at each temperature. The statistical errors are obtained from the mean-square deviation of the time correlation functions. Due to the large statistics in the calculations, the statistical error of the self-diffusion coefficient D is less than 0.1%, while the shear viscosity η and thermal conductivity λ_T has a statistical error of about 1%. The magnitude of the statistical errors can be further reduced by longer simulations if larger computational resources are available.

The results of all transport properties between 300 K and 1000 K are summarized in Table 1. The experimental data [32,33] at different temperatures are also included in Table 1 to compare with the calculated results. The uncertainty of the experimental data was estimated to be 5% for self-diffusion coefficients and 0.9% for shear viscosity [32]. The accuracy of the experimental thermal conductivity of carbon dioxide is estimated to be ±1% near room temperature and ±2% at the higher temperatures [33]. From Table 1 we can see the average deviations between the calculated and experimental values for self-diffusion coefficient and shear viscosity are 2.32%, and 0.71%, respectively. The excellent agreement indicates the linear rigid rotor assumption of the CO_2 molecule is valid even at 1000 K. As shown in Table 1, the calculated thermal conductivities underestimate the experimental values by 2.30% averagely. The deviation can be further reduced if the aharmonic vibrations of molecules are taken into account. Compared to the calculated CO_2 thermal conductivities from other authors who obtained a deviation of 35% without considering the vibrational energies and a deviation of 22% with a classical treatment of the vibrational motions [18], our quantum mechanical treatment of the vibrational energies greatly improves the accuracy of the calculated thermal conductivity. Overall, excellent agreements are achieved for all the three transport properties of interest.

6. Conclusions

The EMD and the time correlation theory are employed in this work to determine the transport properties of CO_2 gas. The calculations demonstrate a procedure of determination of self-diffusion coefficient, shear viscosity and thermal conductivity of a polyatomic gas without using any experimental data. All the parameters used in the calculations such as the C–O bond length, moment of inertia, intermolecular potential and vibrational energy eigen values are determined by *ab initio* method. In order to take into account the quantum effects of molecular vibrations, a MC method is used to initialize the vibrational energies at the given temperature. The good agreement of calculated values with the experimental data validates the rigid rotor and frozen vibrational energy assumptions we made at the beginning of the calculations. Since the vibrational energies do not vary with time in the simulation after they are initialized, the vibrational contribution to the thermal conductivity might be reduced to a simpler form by separating the terms involving the vibrational energies from those involving other energies which vary continuously with time. If this simplification can be achieved, a more efficient calculation of the thermal conductivity will be possible.

The present method can be readily extended to the calculations of transport properties of other gases or gas mixtures which contain monatomic, diatomic or polyatomic molecules at different temperatures as long as the accurate intermolecular potentials are available.

List of symbols

d_{ia} the distance of the site a in the molecule i relative to the center of mass

D	self-diffusion coefficient
$\vec{e}$	the unit vectors along the molecular axis
E_p	total potential energy of the system
E_i	the energy of the molecule i
E_{Vi}	vibrational energy of the molecule i
E_{vj}	the fundamental vibrational transition energy of mode j
$\vec{f}_{ij_\beta}$	a component of the force acting on the molecule i due to the molecule j
$\vec{F}_{ij}$	intermolecular force due to the interaction between the molecule i and the molecule j
$\vec{G}$	$\vec{e} \times \vec{G}$ is the torque acting on the molecule
$\vec{G}^{\perp}$	the component of $\vec{G}$ perpendicular to $\vec{e}$
$\hbar$	reduced Planck constant
I	moment of inertia
J_α	a component of the energy current
k_B	Boltzmann constant
m	the mass of molecule
n_j	the vibrational energy level of jth vibrational mode
N	number of molecules
P	pressure
P_0	the desired pressure
r_{ab}	distance between nuclei a and b
r_0	C–O bond length
r_{AB}	the distance between centers of mass of molecule A and molecule B
r_{cut}	cut-off distance
r_{ij_α}	a component of the distance vector from the molecule j to i
t	time
T	temperature
T_0	the desired temperature
u_i	rotational velocity of the molecule i
U_{BUK}	BUK intermolecular potential
U_{AB}	modified BUK potential
$v_{i\alpha}$	a component of translational velocity of molecule i
V	volume

Greek letters

β_T	isothermal compressibility
η	shear viscosity
λ	scale factor of velocity
λ_T	thermal conductivity
μ	scale factor of intermolecular distance
$P_{\alpha\beta}$	off-diagonal element of pressure tensor
τ_T	time constant for temperature relaxation
τ_p	time constant for pressure relaxation

Acknowledgments

This work was supported by Office of Navy Research through the Multidisciplinary University Research Initiative (MURI) program.

Appendix A.

Derivation of the expression for the energy current

$$J_\alpha = \frac{d}{dt}\left[\frac{1}{V}\sum_i r_{i\alpha}(E_i - \langle E_i\rangle)\right]. \tag{A1}$$

In a constant *NVE* ensemble, volume V and average energy $\langle E_i\rangle$ are both constant.

$$J_\alpha = \frac{1}{V}\left(\sum_i v_{i\alpha}(E_i - \langle E_i\rangle) + \sum_i r_{i\alpha}\frac{dE_i}{dt}\right) = \frac{1}{V}\left(\sum_i v_{i\alpha}E_i + \sum_i r_{i\alpha}\frac{dE_i}{dt}\right). \tag{A2}$$

The total momentum of the system is kept constant during the simulation. The initial value of the total momentum is set to zero so that $\sum_i v_{i\alpha} = 0$. Hence, the term $\sum_i v_{i\alpha}\langle E_i\rangle$ vanishes. The time derivative of E_i is

$$\begin{aligned}\frac{dE_i}{dt} &= m\vec{v}_i\cdot\frac{d\vec{v}_i}{dt} + I\vec{u}_i\cdot\frac{d\vec{u}_i}{dt} + \frac{dE_{Vi}}{dt} + \frac{1}{2}\sum_{j\neq i}\left[\frac{\partial U_{ij}}{\partial\vec{r}_{ij}}\cdot\frac{\partial\vec{r}_{ij}}{\partial t} + \frac{\partial U_{ij}}{\partial\vec{e}_i}\cdot\frac{\partial\vec{e}_i}{\partial t} + \frac{\partial U_{ij}}{\partial\vec{e}_j}\cdot\frac{\partial\vec{e}_j}{\partial t}\right] = \vec{v}_i\cdot\sum_{j\neq i}\vec{F}_{ij} \\ &\quad + \vec{u}_i\cdot\sum_{j\neq i}\vec{G}_{ij}^{\perp} + \frac{1}{2}\sum_{j\neq i}[-\vec{F}_{ij}\cdot(\vec{v}_i - \vec{v}_j) - \vec{G}_{ij}\cdot\vec{u}_i - \vec{G}_{ji}\cdot\vec{u}_j] \\ &= \frac{1}{2}\sum_{j\neq i}[\vec{F}_{ij}\cdot(\vec{v}_i + \vec{v}_j) + \vec{G}_{ij}^{\perp}\cdot\vec{u}_i - \vec{G}_{ji}^{\perp}\cdot\vec{u}_j],\end{aligned} \tag{A3}$$

where $dE_{Vi}/dt = 0$ because the vibrational energy is assumed as frozen in the molecule. The intermolecular potential U_{ij} is not only a function of $\vec{r}_{ij}$, the distance between the centers of mass, but also a function of molecular orientations $\vec{e}_i$ and $\vec{e}_j$. Therefore, the chain rule is used to determine the time derivative of U_{ij}. Note $\vec{G}_{ij}\cdot\vec{u}_i = \vec{G}_{ij}^{\perp}\cdot\vec{u}_i$ since $\vec{u}_i$ is perpendicular to the molecular axis $\vec{e}_i$, and $\vec{G}_{ij}^{\perp}$ is the component of $\vec{G}_{ij}$ perpendicular to $\vec{e}_i$. Therefore, the second summation in Eq. (A2) is

$$\begin{aligned}\sum_i r_{i\alpha}\frac{dE_i}{dt} &= \sum_i r_{i\alpha}\left(\frac{1}{2}\sum_{j\neq i}[\vec{F}_{ij}\cdot(\vec{v}_i + \vec{v}_j) + \vec{G}_{ij}^{\perp}\cdot\vec{u}_i - \vec{G}_{ji}^{\perp}\cdot\vec{u}_j]\right) \\ &= \frac{1}{4}\sum_i\sum_{j\neq i} r_{i\alpha}[\vec{F}_{ij}\cdot(\vec{v}_i + \vec{v}_j) + \vec{G}_{ij}^{\perp}\cdot\vec{u}_i - \vec{G}_{ji}^{\perp}\cdot\vec{u}_j] \\ &\quad + \frac{1}{4}\sum_j\sum_{i\neq j} r_{j\alpha}[\vec{F}_{ji}\cdot(\vec{v}_i + \vec{v}_j) + \vec{G}_{ji}^{\perp}\cdot\vec{u}_j - \vec{G}_{ij}^{\perp}\cdot\vec{u}_i] \\ &= \frac{1}{4}\sum_i\sum_{j\neq i} r_{ij\alpha}[\vec{F}_{ij}\cdot(\vec{v}_i + \vec{v}_j) + \vec{G}_{ij}^{\perp}\cdot\vec{u}_i - \vec{G}_{ji}^{\perp}\cdot\vec{u}_j] \\ &= \frac{1}{2}\sum_i\sum_{j>i} r_{ij\alpha}[\vec{F}_{ij}\cdot(\vec{v}_i + \vec{v}_j) + \vec{G}_{ij}^{\perp}\cdot\vec{u}_i - \vec{G}_{ji}^{\perp}\cdot\vec{u}_j],\end{aligned} \tag{A4}$$

where $\vec{F}_{ij} = -\vec{F}_{ji}$ according to Newton's third law and $r_{ij\alpha} = r_{i\alpha} - r_{j\alpha}$. Note $\vec{G}_{ij}^{\perp} \neq -\vec{G}_{ji}^{\perp}$. Comparing Eq. (A4) to the second term of Eq. (6), one gets

$$\frac{dE_{ij}}{dt} = \frac{1}{2}(\vec{v}_i + \vec{v}_j)\cdot\vec{F}_{ij} + \frac{1}{2}(\vec{u}_i\cdot\vec{G}_{ij}^{\perp} - \vec{u}_j\cdot\vec{G}_{ji}^{\perp}). \tag{A5}$$

References

[1] B. Eckl, J. Vrabec, H. Hasse, Fluid Phase Equilib. 274 (2008) 16–26.
[2] X. Li, L. Zhao, T. Cheng, L. Liu, H. Sun, Fluid Phase Equilib. 274 (2008) 36–43.
[3] G.A. Fernandez, J. Vrabec, H. Hasse, Mol. Simul. 31 (2005) 787–793.
[4] G.A. Fernandez, J. Vrabec, H. Hasse, Fluid Phase Equilib. 221 (2004) 157–163.
[5] F. Case, A. Chaka, D.G. Friend, D. Frurip, J. Golab, J. Rusel, J. Moore, R.D. Mountain, J. Olson, M. Schiller, J. Store, Fluid Phase Equilib. 217 (2004) 1–10.
[6] Z. Liang, H.L. Tsai, J. Mol. Spectrosc. 252 (2008) 108–114.
[7] G. Granar, C. Rosseti, D. Bailly, Mol. Phys. 58 (1986) 627–636.
[8] R. Bukowski, J. Sadlej, B. Jeziorski, P. Jankowski, K. Szalewicz, S.A. Kucharski, H.L. Williams, B.M. Rice, J. Chem. Phys. 110 (1999) 3785–3803.

[9] G. Steinebrunner, A.J. Dyson, B. Kirchner, H. Huber, J. Chem. Phys. 109 (1998) 3153–3159.
[10] S. Bock, E. Bich, E. Vogel, Chem. Phys. 257 (2000) 147–156.
[11] M.S. Green, J. Chem. Phys. 19 (1951) 1036–1046.
[12] M.S. Green, Phys. Rev. 119 (1960) 829–830.
[13] R. Kubo, J. Phys. Soc. Jpn. 12 (1957) 570–586.
[14] M.P. Allen, D.J. Tildesley, Computer Simulation of Liquids, Clarendon Press, Oxford, 2000.
[15] D. Evans, Phys. Rev. A 34 (1986) 1449–1458.
[16] D.M. Heyes, Phys. Rev. B 37 (1988) 5677–5696.
[17] F. Müller-Plathe, J. Chem. Phys. 106 (1997) 6082–6085.
[18] C. Nieto-Draghi, T. de Bruin, J. Perez-Pellitero, J.B. Avalos, A.D. Mackie 126 (2007) 064509.
[19] K.P. Travis, D.J. Searles, D.J. Evans, Mol. Phys. 95 (1998) 195–202.
[20] J.G. Harris, K.H. Yung, J. Phys. Chem. 99 (1995) 12021–12024.
[21] C. Bratschi, H. Huber, D.J. Searles, J. Chem. Phys. 126 (2007) 164105.
[22] Z. Zhang, Z. Duan, J. Chem. Phys. 122 (2005) 214507.
[23] R. Zwanzig, N.K. Ailawadi, Phys. Rev. 182 (1969) 280–283.
[24] E. Helfand, Phys. Rev. 119 (1960) 1–9.
[25] S. Viscardy, J. Servantie, P. Gaspard, J. Chem. Phys. 126 (2007) 184513.
[26] C. Leonard, M. Diehr, P. Rosmus, W.C. Maguire, JQSRT 109 (2008) 535–548.
[27] D. Frenkel, B. Smit, Understanding Molecular Simulation, Academic Press, San Diego/San Francisco/New York/Boston/London/Sydney/Tokyo, 2002.
[28] H.J.C. Berendsen, J.P.M. Postma, W.F. Van Gunsteren, A. DiNola, J.R. Haak, J. Chem. Phys. 81 (1984) 3684–3690.
[29] K. Singer, A. Taylor, J.V.L. Singer, Mol. Phys. 33 (1977) 1757–1795.
[30] K. Meier, A. Laesecke, S. Kabelac, J. Chem. Phys. 121 (2004) 3671–3687.
[31] S. Hess, D.J. Evans, Phys. Rev. E 64 (2001) 011207.
[32] A. Boushehri, J. Bzowski, J. Kestin, E.A. Mason, J. Phys. Chem. Ref. Data 17 (1988) 255.
[33] V. Vesovic, W.A. Wakeham, G.A. Olchowy, J.V. Sengers, J.T.R. Watson, J. Millat, J. Phys. Chem. Ref. Data 19 (1990) 763–808.